International Journal of Power and Energy Systems, Vol. 46, No. 10, 2026
An Open Access Paper

FAULT DIAGNOSIS OF PHOTOVOLTAIC POWER SYSTEMS BASED ON DEEP LEARNING TECHNOLOGY

Yu Li,* Dingwen Hu,** and Rui Yang***

Abstract

This paper briefly introduces the generative adversarial network (GAN) algorithm for enhancing fault training samples and the convolutional neural network (CNN) algorithm for diagnosing faults in photovoltaic arrays. Simulation experiments were conducted. Photovoltaic array equipment was used to collect actual photovoltaic array fault data. Then, the GAN algorithm was used to enhance the sample data, and the performance of the GAN algorithm was indirectly evaluated using the CNN algorithm. Finally, it was compared with the support vector machine and back-propagation neural network (BPNN) algorithms. The results showed that the GAN algorithm could effectively enhance small sample data and the CNN algorithm could diagnose faults in photovoltaic arrays more accurately. Feature indicators such as output current, output voltage, load voltage, and load current were important for diagnosing the types of faults in photovoltaic arrays. The novelty of this paper lies in using the GAN algorithm to enhance the fault sample data, so as to solve the problem of the lack of high-quality photovoltaic fault data in reality, and using the CNN algorithm to identify photovoltaic faults.

Key Words

Photovoltaic array, fault diagnosis, GAN, CNN

1. Introduction

In the context of the accelerated transition of the global energy structure towards low-carbon and clean energy, photovoltaic power generation, as an important component of renewable energy, is playing an increasingly crucial role in promoting green and sustainable development, alleviating the pressure on traditional fossil energy and responding to climate change [1]-[2]. However, the operating environment of photovoltaic power systems is complex and changeable, affected by various factors such as light intensity, temperature changes, dust shielding, component aging, and inverter failure [3]-[4]. Traditional photovoltaic system fault diagnosis methods mainly rely on physical model analysis or manual experience judgment. Although these methods can identify some typical faults to a certain extent, they often have slow response speed, low diagnostic accuracy, and difficulty adapting to complex working conditions [5]. In this context, deep learning technology, with its nonlinear modeling ability, feature self-learning ability, and generalization ability, provides new ideas and technical approaches for solving the problem of fault diagnosis of photovoltaic systems. Deep learning builds multi-layer neural network models to automatically extract complex latent features from massive historical data and thereby establish nonlinear mapping relationships between input variables and fault types [6]. Fan et al. [7] proposed a photovoltaic grid-connected modeling method based on the RTDS software platform and analyzed the effects of light intensity and ambient temperature on photovoltaic grid-connected systems. Zhang et al. [8] presented a residual learning-based unmanned aerial vehicle (UAV) image analysis model for fault identification and location in low-voltage distributed photovoltaics. Chen et al. [9] presented a pre-diagnosis method for photovoltaic array faults based on current-voltage conversion, type identification, and degree diagnosis. The above relevant studies have all analyzed the photovoltaic system. Some of them focused on the grid connection problem of the photovoltaic system, while others focused on using intelligent algorithms to detect photovoltaic system faults. Their shortcoming is failing to effectively solve the problem of insufficient fault samples in training sets. This paper also focuses on the identification and detection of photovoltaic system faults, and emphasizes on solving the problem of the lack of high-quality photovoltaic fault data samples in reality. This paper used the generative adversarial network (GAN) algorithm to generate photovoltaic fault samples, thereby improving sample quality and enhancing the training performance of the convolutional neural network (CNN) al-

* Xi'an University of Architecture and Technology, China; e-mail: lyu_liy@hotmail.com
** Xi'an Jiaotong University, China; e-mail: hdw_hu@outlook.com
*** Northwestern Polytechnical University, China; e-mail: yr_yang@hotmail.com
Corresponding author: Yu Li

(DOI: 10.2316/J.2026.203-0643)

gorithm. Finally, the CNN algorithm was used to identify photovoltaic system faults. This paper briefly introduces the GAN algorithm for enhancing fault training samples and the CNN algorithm for diagnosing faults in photovoltaic arrays, followed by simulation experiments. The GAN algorithm was used to augment the sample data of dynamic shadow occlusion, static shadow occlusion, and open circuit faults, i.e., expanding these small-scale samples, so as to provide larger-scale and more balanced training samples for subsequent CNN training and avoid algorithm overfitting. The contribution of this paper lies in providing an effective reference for improving the accuracy of CNNs in detecting faults in photovoltaic systems by using the GAN algorithm to enhance the training sample data.

2. Fault Diagnosis of Photovoltaic Power Systems Based on Deep Learning

The various subsystems of a photovoltaic power system may face different types of faults, and the forms of their fault characteristics may also vary greatly. The parameter indicators required to identify the fault types are also diverse [10]. Considering all the faults and aggregating all parameter indicators into one algorithm to make a single algorithm applicable to fault diagnosis of all subsystems will not only make the training of the algorithm complex. Moreover, the fault features of different subsystems can interfere with each other, resulting in reduced accuracy of the algorithm [11], [12]. Therefore, this paper focuses on photovoltaic module arrays and uses deep learning algorithms to diagnose faults in photovoltaic arrays [13], [14].

2.1 Fault Sample Data Augmentation

In this paper, deep learning technology is used to identify faults in photovoltaic arrays. Its principle is to use the fault data of photovoltaic arrays to train deep learning models [15] and use the nonlinear mapping patterns obtained from training to diagnose the fault types of photovoltaic arrays. For deep learning models, high-quality training data is crucial, but in practical applications, photovoltaic arrays need to be stable enough before connecting to the grid, so the amount of photovoltaic array fault data that can be obtained is relatively small [16]. To address the problem of small sample size of photovoltaic array failure data, the GAN algorithm is used to expand the sample size.

GAN consists of a generator and a discriminator. A segment of Gaussian distributed noise data is input into the generator. After forward computation in the hidden layer within the generator, a segment of generated data is obtained. Then, the generated data is mixed with the actual sampled photovoltaic array fault data and input into the discriminator to determine whether the input data is a real fault. The parameters of the discriminator and the generator are adjusted based on the loss function of the judgment result until the discriminator cannot distinguish the actual sampled data from the generated data given by the gener-

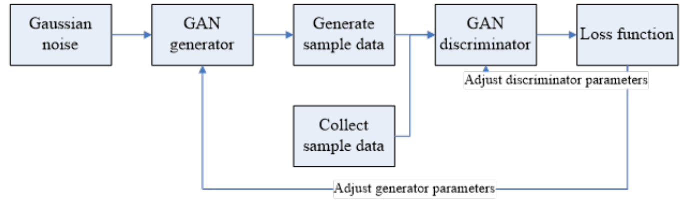

Figure 1. The Training Process of The GAN Algorithm

ator. The generated data can be used as enhanced sample data for subsequent training [17]. The specific training process of the GAN (Figure 1) is shown below.

(1) A segment of random noise data that conforms to a Gaussian distribution is randomly generated.
(2) The noise is input into the GAN generator for forward computation. The GAN generator uses a three-layer gated recurrent unit (GRU) structure. The reason for using GRU is that, compared with LSTM, it has a simpler structure, which can improve the operation speed. Meanwhile, the performance difference between them is not significant. The forward computation formula of the GRU is:

$$\left\{\begin{array}{l} z_t=f\left(\omega_z\left(h_{t-1}, x_t\right)\right) \\ r_t=f\left(\omega_r\left(h_{t-1}, x_t\right)\right) \\ h_t=\tanh \left(\omega\left(r_t \times h_{t-1}, x_t\right)\right) \\ h_t=\left(1-z_t\right) \times h_{t-1}+z_t \times h_t^{\prime} \end{array}\right. \tag{1}$$

where z_t is the update gate output, r_t is the output of the reset gate [18], ω_z and ω_T are the weight in the update gate and reset gate, x_t is the current input, $f()$ is the activation function, h_{t-1} is the hidden state of the previous moment, h_t is a temporary hidden state at the present moment, ω is the weight when calculating h_t, and h_t is the hidden state at the current moment.
(3) The generated data obtained by the forward computation of the GAN generator and the same amount of actual fault sampling data are input into the GAN discriminator for authenticity determination [19]. The GAN discriminator adopts a convolutional structure and uses convolutional kernels to extract convolutional features from the input data. The probability that the input data is real fault data is calculated based on the convolutional features in the fully connected layer, and the judgment results are output in the output layer.
(4) Whether the GAN training has been terminated is determined. If the number of training sessions reaches the preset number or the loss function converges to a stable state, the training stops. Otherwise, the parameters in the generator and discriminator are adjusted reversely according to the loss function. The formula for the loss function is:

$$\begin{aligned} \text{loss } =&\frac{1}{2} \sum_x p(x) \log \left(\frac{2 p(x)}{p(x)+q(x)}\right) \\ & +\frac{1}{2} \sum_x q(x) \log \left(\frac{2 q(x)}{p(x)+q(x)}\right) \end{aligned} \tag{2}$$

where $p(x)$ is the distribution of the probability that the input data is real fault data, calculated by the discrimina-

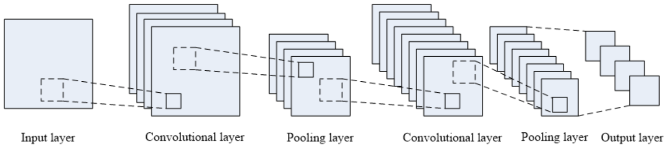

Figure 2. The Basic Architecture of CNN

tor and $q(x)$ is the probability distribution of the actual real fault data.

2.2 The CNN-Based Photovoltaic Fault Diagnosis Algorithm

When monitoring faults in photovoltaic arrays, whether the operation is normal is determined by collecting changes in various indicators over a certain period. That is to say, the collected sample data is the curve of changes in feature indicators over a period of time. Load voltage, inverter current, irradiance, inverter voltage, output voltage, output current, ambient temperature, and load current are used as feature indicators for diagnosing faults in photovoltaic arrays, and these indicators can all be collected using the corresponding sensors. In the face of the variation graphs of various feature indicators, the CNN algorithm is used to diagnose photovoltaic faults, and the process is as follows.

(1) A trained GAN generator is employed to produce training samples of different fault types.

(2) The variation curve graph of the feature indicators of the training samples are input into the CNN. Convolutional features are extracted using convolution kernels in the convolutional layer. The convolution formula is:

$$y = f\left(\sum_{\bar{i},j}(x \otimes w)_{\bar{i},j} + b\right) \tag{3}$$

where y is the convolutional feature output by the convolutional layer [20], x is the input sample, w is a convolution kernel, b is a bias, and $f()$ is the activation function. The convolutional features extracted are compressed in the pooling layer, and the pooling box slides over the extracted convolutional feature map. Each slide compresses the feature data within the pooling box. In this paper, max-pooling is used, i.e., the maximum value within the pooling box is taken as the compression result.

Convolutional and pooling layers can be set in terms of quantity and order as required.

(3) Forward computations are performed on the compressed convolutional features in the fully connected layer to determine the type of fault.

(4) Whether the training of the CNN algorithm is terminated is determined. The training is stopped if the number of training sessions reaches the threshold or the loss function converges to stability; otherwise, the parameters in the CNN algorithm are reversely adjusted according to the calculation results of the loss function, and return to step 2. Since the CNN algorithm adopted in this paper is used for diagnosing the types of faults in photovoltaic arrays, i.e., it is a classification algorithm, cross-entropy is used as the loss function.

3. Simulation Experiment

3.1 Experimental Data

Some of the photovoltaic array failure sample data used in the simulation experiment were obtained from actual photovoltaic arrays in the photovoltaic microgrid, and the other part was generated by performing data augmentation on the photovoltaic array failure data using the GAN algorithm. The relevant parameters of the photovoltaic array for which the fault samples were collected are as follows. The overall equipment specification was 0.8 m $\times$ 0.4 m $\times$ 0.8 m. The maximum operating voltage and current of the photovoltaic cell was 16.8 V and 0.3 A. The storage battery had a rated voltage of 14 V and a rated current of 3 A. The detection range of the irradiance sensor was 0-2,000 W/m^2. The direct-current input voltage and alternate-current output voltage of the Inverter was 12 V and 220 V (50 Hz). The detection range of the temperature sensor was 0-60°C.

3.2 Experimental Methods

First, actual photovoltaic array failure data were collected. During the collection process, four working states were set for the photovoltaic array equipment: normal working state, dynamic shadow occlusion state, static shadow occlusion state, and open circuit fault. The normal working state refers to the situation when there is plenty of sunlight and no shading. The dynamic shadow occlusion state refers to a condition where, based on normal operation, foam boards are moved randomly 0.5 meters above the photovoltaic array (ensuring their shadows fall within the photovoltaic array's receiving range) to simulate the shading effects of dynamic obstructions such as passing clouds or tall buildings. The static shadow occlusion refers to a state where, under normal operating conditions, multiple opaque circular paper sheets with a radius of 1 cm are placed on the surface of the photovoltaic array to simulate long-term partial shading caused by factors such as bird droppings or dust accumulation. An open circuit fault refers to the disconnection of some of the photovoltaic cells in the photovoltaic array on the basis of normal operation. When collecting data, four identical photovoltaic array devices were prepared and operated under the above four working conditions from 11 a.m. to 1 p.m. in good weather. The load voltage, inverter current, irradiance, inverter voltage, output voltage, output current, ambient temperature, and load current of the four devices were collected during this period. Then, the collected data was divided at intervals of ten seconds, and 720 samples were obtained, of which 180 were normal samples, 180 were dynamic local shadow faults, 180 were static local shadow faults, and 180 were open circuit faults.

Table 1
Performance Test Results of the GAN Algorithm

Fault status	Not using GAN			Using GAN		
	P	R	F	P	R	F
Normal sample	0.498 ± 0.012	0.486 ± 0.010	0.487 ± 0.008	0.755 ± 0.011	0.721 ± 0.012	0.737 ± 0.011
Dynamic shadow occlusion	0.294 ± 0.011	0.286 ± 0.008	0.287 ± 0.007	0.754 ± 0.010	0.722 ± 0.011	0.736 ± 0.012
Static shadow occlusion	0.356 ± 0.010	0.348 ± 0.009	0.351 ± 0.009	0.755 ± 0.011	0.723 ± 0.010	0.736 ± 0.010
Open circuit fault	0.289 ± 0.011	0.269 ± 0.010	0.274 ± 0.010	0.756 ± 0.010	0.725 ± 0.010	0.737 ± 0.011
Average	0.359 ± 0.012	0.347 ± 0.011	0.350 ± 0.011	0.755 ± 0.011	0.723 ± 0.011	0.737 ± 0.012

In the GAN generator, there was a three-layer GRU with 128 hidden nodes, and the activation function was sigmoid. In the GAN discriminator, Convolutional layer 1 contained 32 convolutional kernels (3×3), with a step length of 2, and used the sigmoid activation function; Convolutional layer 2 contained 64 convolution kernels (3×3), with a step length of 2, and used the sigmoid activation function; a 3×3 max-pooling box was used in the pooling layer, with a step length of 2; the fully connected layer adopted the softmax function.

The structure of the CNN algorithm was an input layer - Convolutional layer 1 - Convolutional layer 2 - Pooling layer 1 - Convolutional layer 3 - Pooling layer 2 - a fully connected layer - an output layer. The input layer had a specification of 200×250. Convolutional layer 1 contained 32 convolution kernels (2×2), with a step length of 1, and used the sigmoid activation function; Convolutional layers 2 and 3 each contained 64 convolution kernels (2×2), with a step length of 1, and used the sigmoid activation function. Within Pooling layers 1 and 2, there was a 2×2 max-pooling box, and the step length was 1. The fully connected layer used the softmax function. In addition, the CNN algorithm was compared with the support vector machine (SVM) and back-propagation neural network (BPNN) algorithms.

3.3 Evaluation Indicators

The performance of the GAN algorithm in generating fault sample data was mainly evaluated indirectly by evaluating the performance of the CNN algorithm trained with generated samples. The equations are:

$$\left\{\begin{array}{l} P=\frac{TP}{TP+FP} \\ R=\frac{TP}{TP+FP} \\ F=\frac{2 \cdot P \cdot R}{P+R} \end{array}\right. \tag{4}$$

where P is the precision, R is the recall rate, F is the combined value of precision and recall rate, TP indicates the number of true positive cases, FP indicates the number of false positive cases, FN indicates the number of false negative cases, and TN represents the number of true negative cases.

Comparisons between the CNN algorithm and the SVM and BPNN algorithms also used the above indicators. In addition, this paper used the Shapley additive explanations (SHAP) method to test the importance of the input feature indicators, and the relevant equations are:

$$\left\{\begin{array}{l} f_X(S)=E\left[f(X) \mid X_S\right] \\ \Delta i(S)=f_X(S \cup\{i\})-f_X(S) \\ \phi_i=\sum_S \frac{|S|!(N-|S|-1)!}{N!} \cdot \Delta i(S) \\ g(x)=\phi_0+\sum_{i=1}^p \phi_i \cdot z_i \end{array}\right. \tag{5}$$

where X is the collection of input samples, each of which has N features, S is a subset of sample feature set N that does not contain feature $i, f_X(S)$ is the expected value of the output of $S, \Delta i(S)$ represents the marginal contribution of feature i added to S in the model prediction results, ϕ_i is the SHAP value of feature $i, g(x)$ is the constructed feature contribution explanation function, ϕ_0 is the base value, which is the mean of the predicted model results, and z_i is an indicative parameter that takes a value of 1 when the feature is present and zero otherwise. For example, when calculating the contribution of feature i, only z_i takes a value of 1 , and the rest of the values are 0.

3.4 Experimental Results

The sample data generated by the GAN algorithm was used to train the CNN algorithm, and then it was compared with the CNN algorithm trained with actually collected small samples to indirectly evaluate the performance of the GAN algorithm. It can be seen from Table 1 that the overall performance of the CNN algorithm trained without samples generated by the GAN algorithm was weaker than that of the CNN trained with samples generated by the GAN algorithm. In addition, the diagnostic performance of the former varied when dealing with different types of faults, while the former showed no significant difference.

The SVM, BPNN, and CNN algorithms were trained and tested using the sample data enhanced by the GAN algorithm. It can be seen from Table 2 that there was little difference in the performance of the three algorithms in diagnosing different types of faults after training with samples whose data was enhanced by the GAN algorithm, indicating that the data augmentation function of the GAN algorithm was also applicable to other classification algorithms. In comparison of the same fault types and average performance, the CNN algorithm performed the best, followed by the BPNN algorithm, and the SVM algorithm performed the worst.

In order to verify the diagnostic performance of the proposed algorithm for photovoltaic faults under noise interference, Gaussian noise was added to the original samples. Then, the SVM, BPNN, and the CNN algorithm underwent diagnostic tests, and the F value was adopted to

Table 2
Fault Diagnosis Performance of Different Algorithms

Fault type	Evaluation indicator	SVM	BPNN	CNN
Normal sample	P	0.555 ± 0.021	0.711 ± 0.014	0.755 ± 0.008
	R	0.521 ± 0.022	0.682 ± 0.013	0.721 ± 0.007
	F	0.532 ± 0.021	0.698 ± 0.014	0.737 ± 0.009
Dynamic shadow occlusion	P	0.554 ± 0.023	0.712 ± 0.013	0.754 ± 0.010
	R	0.523 ± 0.021	0.687 ± 0.012	0.722 ± 0.011
	F	0.535 ± 0.022	0.697 ± 0.014	0.736 ± 0.010
Static shadow occlusion	P	0.556 ± 0.023	0.715 ± 0.015	0.755 ± 0.008
	R	0.524 ± 0.024	0.685 ± 0.016	0.723 ± 0.009
	F	0.537 ± 0.021	0.696 ± 0.013	0.736 ± 0.010
Open circuit fault	P	0.557 ± 0.023	0.716 ± 0.012	0.756 ± 0.008
	R	0.526 ± 0.022	0.685 ± 0.011	0.725 ± 0.010
	F	0.538 ± 0.023	0.696 ± 0.015	0.737 ± 0.008
Average	P	0.559 ± 0.024	0.714 ± 0.014	0.755 ± 0.007
	R	0.523 ± 0.023	0.687 ± 0.016	0.723 ± 0.009
	F	0.538 ± 0.021	0.697 ± 0.014	0.737 ± 0.010

Table 3
The F Value of the Diagnostic Performance of Algorithms Before and After Adding Noise To the Samples

Fault type	Interference	SVM	BPNN	CNN
Normal sample	No noise added	0.532 ± 0.021	0.698 ± 0.014	0.737 ± 0.009
	Noise added	0.503 ± 0.023*	0.691 ± 0.011*	0.736 ± 0.008
Dynamic shadow occlusion	No noise added	0.535 ± 0.022	0.697 ± 0.014	0.736 ± 0.010
	Noise added	0.502 ± 0.023*	0.690 ± 0.012*	0.735 ± 0.009
Static shadow occlusion	No noise added	0.537 ± 0.021	0.696 ± 0.013	0.736 ± 0.010
	Noise added	0.506 ± 0.023*	0.688 ± 0.016*	0.735 ± 0.011
Open circuit fault	No noise added	0.538 ± 0.023	0.696 ± 0.015	0.737 ± 0.008
	Noise added	0.502 ± 0.020*	0.687 ± 0.016*	0.736 ± 0.009
Average	No noise added	0.538 ± 0.021	0.697 ± 0.014	0.737 ± 0.010
	Noise added	0.501 ± 0.023*	0.687 ± 0.017*	0.736 ± 0.011

Note: $*$ indicates significant at the 5% level.

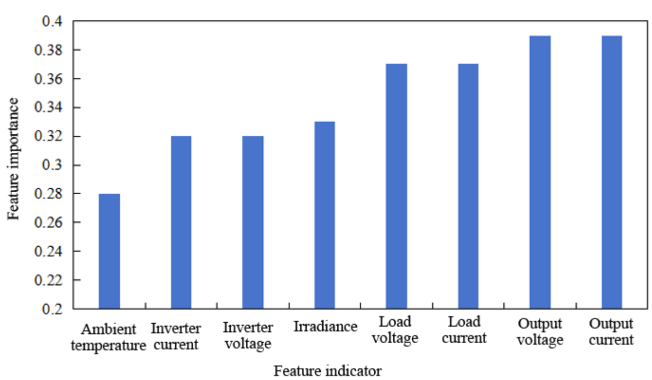

Figure 3. The Feature Importance in the Proposed Photovoltaic Array Fault Diagnosis Algorithm

measure the performance. The results are shown in Table 3. It can be seen that after adding Gaussian noise to the test samples, the diagnostic performance of both the SVM and BPNN algorithms decreased significantly, while that of the CNN algorithm did not change significantly.

The SHAP algorithm calculated the feature importance in the proposed photovoltaic array fault diagnosis algorithm. It can be seen from Figure 3 that for diagnosing the type of photovoltaic array fault, the feature indicators such as output current, output voltage, load voltage, load current were relatively important, followed by irradiance, inverter current, and inverter voltage, and the ambient temperature was the least important. Reasons for the above results are analyzed. Under normal circumstances, the structure of photovoltaic modules is stable. Even if the environmental temperature changes, as long as there is no drastic temperature change in a short period, it will not have a serious impact on photovoltaic modules. Inverter current and voltage convert the direct current generated by photovoltaic modules into alternating current through an inverter. Abnormalities in inverter current and voltage may also be due to a malfunction of the inverter. Output current, output voltage, load voltage, and load current are directly related to photovoltaic modules and can more directly reflect the overall problems of photovoltaic modules.

4. Conclusions

Facing the problem of small sample size in the training of photovoltaic fault identification algorithms, this paper introduced the GAN algorithm to increase fault sample size and the CNN algorithm to diagnose faults in photovoltaic arrays. Simulation experiments were conducted. Photovoltaic array equipment was used to collect actual photovoltaic array fault data. Then, the GAN algorithm was used to enhance the sample data, and the performance of the GAN algorithm was indirectly evaluated using the CNN algorithm. Finally, it was compared with the SVM and BPNN algorithms. It was found that the GAN algorithm could effectively enhance the sample data and improve the diagnostic performance of the CNN algorithm. The data augmentation function of the GAN algorithm was also applicable to other classification algorithms, and the diagnostic performance of the CNN algorithm was the best, followed by the BPNN algorithm, and the SVM algorithm was the worst. Moreover, the CNN algorithm exhibited the superior performance in resisting noise interference. Feature indicators such as output current, output voltage, load voltage, and load current were important for diagnosing the types of faults in photovoltaic arrays.

One of the limitations of this paper is the small scale and scope of the samples used in the tests, which results in a low generalization of the test results. Moreover, there has been no sufficient research on the setting of hyperparameters and their convergence. Therefore, future research will expand the scope and scale of the samples, broaden the setting range of hyperparameters and analyze their convergence, and apply them to the real working environment.

Funding Source(s)

The study was supported by 2025 Annual University-level Scientific Research Project "Research on Photovoltaic Array Fault Diagnosis Based on Generative Adversarial Networks and Convolutional Neural Networks" (Project No. KZ25SYYB04).

References

[1] J. Gao, K. O. Asamoah, E. B. Sifah, A. Smahi, and Q. Xia, "Gridmonitoring: Secured sovereign blockchain based monitoring on smart grid," *IEEE Access*, vol. 6, no. 99, pp. 9917–9925, 2018.

[2] U. C. Turhal, Y. Onal, and K. Turhal, "Enhanced fault detection and diagnosis in photovoltaic arrays using a hybrid nca-cnn model," *CMES-Computer Modeling in Engineering & Sciences*, vol. 143, no. 2, pp. 2307–2332, 2025.

[3] T. Kamel, Y. Biletskiy, and L. Chang, "Fault diagnosis and online monitoring for grid-connected single-phase inverters," *Electric Power Systems Research*, vol. 126, pp. 68–77, 2015.

[4] P. Dutta and M. Majumder, "An improved grey wolf optimization technique for estimation of solar photovoltaic parameters," *International Journal of Power and Energy Systems*, vol. 41, pp. 217–221, 2021.

[5] H. Fu, H. Liu, S. Xie, S. Liu, H. Han, and J. Ma, "Multi-coupling fault detection and diagnosis of photovoltaic arrays with improved slime mould algorithm and polycatboost," *Process Safety and Environmental Protection*, vol. 194, pp. 523–541, 2025.

[6] G. C. Madueño, J. J. Nielsen, D. M. Kim, N. Pratas, Č. Stefanović, and P. Popovski, "Assessment of lte wireless access for monitoring of energy distribution in the smart grid," *IEEE Journal on Selected Areas in Communications*, vol. 34, no. 3, pp. 675–688, 2015.

[7] F. Hong and M. Lian, "Method of photovoltaic and network access systems to voltage stability based on typical faults," in *2016 IEEE 11th Conference on Industrial Electronics and Applications (ICIEA)*, pp. 2536–2540, IEEE, 2016.

[8] X. Zhang, Y. Ge, Y. Wang, J. Wang, W. Wang, and L. Lu, "Residual learning-based robotic image analysis model for low-voltage distributed photovoltaic fault identification and positioning," *Frontiers in Neurorobotics*, vol. 18, pp. 1–14, 2024.

[9] X. Chen, M. Jiang, K. Ding, Z. Yang, J. Zhang, L. Cui, and H. M. Hasanien, "Fault prediagnosis, type identification, and degree diagnosis method of the photovoltaic array based on the current–voltage conversion," *IEEE Transactions on Power Electronics*, vol. 39, no. 12, pp. 16708–16719, 2024.

[10] T. Yang and W. Gui, "Research on multi-objective coordinated control strategies of grid-connected inverter under unbalanced voltage conditions," *Diangong Jishu Xuebao/Transactions of China Electrotechnical Society*, vol. 30, no. 11, pp. 148–157, 2015.

[11] I. Ashfaq, Z. Uddin, and N. U. Islam, "Fault diagnosis and localization in photovoltaic-fed cascaded half-bridge five-level inverter using residual network architecture," *Electrical Engineering*, vol. 107, no. 10, pp. 12861–12884, 2025.

[12] X. Chi, D. Wei, M. Shen, and Y. He, "A fault diagnosis method for cracks of photovoltaic modules based on calculation of equivalent circuit model parameters," *Solar Energy*, vol. 283, pp. 1–9, 2024.

[13] F. Wu, B. Sun, J. Duan, and K. Zhao, "Online variable topology-type photovoltaic grid-connected inverter," *IEEE Transactions on Industrial Electronics*, vol. 62, no. 8, pp. 4814–4822, 2015.

[14] B. Wang, Y. Xu, Z. Shen, J. Zou, C. Li, and H. Liu, "Current control of grid-connected inverter with lcl filter based on extended-state observer estimations using single sensor and achieving improved robust observation dynamics," *IEEE Transactions on Industrial Electronics*, vol. 64, no. 7, pp. 5428–5439, 2017.

[15] M. Bougoffa, S. Benmoussa, M. Djeziri, and O. Palais, "Hybrid deep learning for fault diagnosis in photovoltaic systems," *Machines*, vol. 13, no. 5, p. 378, 2025.

[16] F. Wu, X. Li, F. Feng, and H. B. Gooi, "Modified cascaded multilevel grid-connected inverter to enhance european efficiency and several extended topologies," *IEEE Transactions on Industrial Informatics*, vol. 11, no. 6, pp. 1358–1365, 2017.

[17] X. Luo, "Design and implementation of wireless voltage monitoring system based on zigbee," *Chinese Journal of Electron Devices*, vol. 12, no. 3, pp. 83–96, 2017.

[18] J. Sharma, P. P. Bhattacharya, and M. K. Jha, "Performance analysis of ieee 802.15.4 in different nlos environments of smart grids," *International Journal of Sensors Wireless Communications & Control*, vol. 6, no. 3, pp. 216–220, 2016.

[19] A. Ortega, C. M. Schweitzer, A. A. Shinoda, and A. V. Ortega, "Simulation of the dnp3 protocol over tcp/ip on a network ieee 802.11g ad-hoc with smart meter," in *2016 IEEE Andescon*, IEEE, 2016.

[20] A. Ortega, A. A. Shinoda, C. M. Schweitzer, F. Granelli, A. V. Ortega, and F. Bonvecchio, "Proposal dnp3 protocol simulation on ns-2 in ieee 802.11g wireless network ad hoc over tcp/ip in smart grid applications," in *2015 IEEE PES Innovative Smart Grid Technologies Latin America (ISGT LATAM)*, IEEE, 2015.

Biographies

Yu Li, received their master's degree from Xi'an University of Architecture and Technology in June 2018. Since then, they have been a Lecturer with Xi'an Siyuan University. Their research interests include photovoltaic power generation and fault analysis.

Dingwen Hu, received their master's degree from Xi'an Jiaotong University in July 2015. Since then, they have been an Engineer with Xi'an Jiaotong University. Their research interests include HVDC flexible systems and new electricity systems.

Rui Yang, received their master's degree from Northwestern Polytechnical University in March 2013. Since then, they have been a Senior Experimentalist with Xi'an University of Architecture and Technology. Their research interests include radar data processing and artificial intelligence.